

Interactive Measuring and Modeling of Cataracts

Abstract

We introduce a novel interactive method to assess cataracts in the human eye by crafting an optical solution that measures the perceptual impact of forward scattering on the foveal region. Current solutions rely on highly-trained clinicians to check the back scattering in the crystallin lens and test their predictions on visual acuity tests. Close-range parallax barriers create collimated beams of light to scan through sub-apertures scattering light as it strikes a cataract. User feedback generates maps for opacity, attenuation, contrast and local point-spread functions. The goal is to allow a general audience to operate a portable high-contrast light-field display to gain a meaningful understanding of their own visual conditions. User evaluations and validation with modified camera optics were performed. Compiled data is used to reconstruct the cataract-affected view of an individual, offering a unique approach for capturing information for screening, diagnostic, and clinical analysis.

1 Introduction

Cataracts are the leading cause of avoidable blindness worldwide. We propose an interactive and compact solution, which goes beyond traditional cataract evaluation procedures by taking advantage of forward scattering to compute maps for opacity, attenuation, contrast, and point-spread function of cataracts. Self-evaluation methods are not intended to replace the need for further clinical assessments. Instead, the dissemination of devices with the ability to estimate intrinsic parameters of the eye may drive the development of future user-sensible technology for displays, rendering techniques, and improve our understanding of the human visual experience.

Cataracts are generally detected subjectively by locating a white reflex during a slit lamp examination. Research tools range from high-end Shack-Hartmann [Donnelly et al. 2004] and femtosecond optical coherence tomography systems, [Palanker et al. 2010] to retro-illuminated image processing techniques [Campanini et al. 2000]. Our approach uses modified parallax barriers to create collimated beams of light to scan the crystallin lens. Placed close to the viewers' eye, the device ensures the beams are projected onto the fovea. These beams scatter when the light path hits a cataract. Patient-centric interactive approach, coupled with a simple optical setup, create four comprehensive measurement maps. To verify their accuracy and precision, we cross-reference our results utilizing user studies and modified camera optics with partially masked diffusers. We reconstruct the cataract-affected view of an individual, offering a unique approach for capturing information for screening, diagnostic testing, and clinical analysis. To the best of our knowledge, this is the first method to interactively measure a local point spread function map of an eye.

1.1 Contributions

We propose an optical design combined with interactive techniques to measure scattering (cataracts) based on a view-dependent high-contrast display. This approach relies on **forward scattering** and interactively computes local PSFs of the crystallin lens. The solution scans the lens without distracting the users' visual point of reference by **creating a static image in the foveal region**. This eliminates the need to track or control the gaze, as current interactive techniques require. Contributions of this paper include:

- A co-design of optics and user interaction that creates an ef-

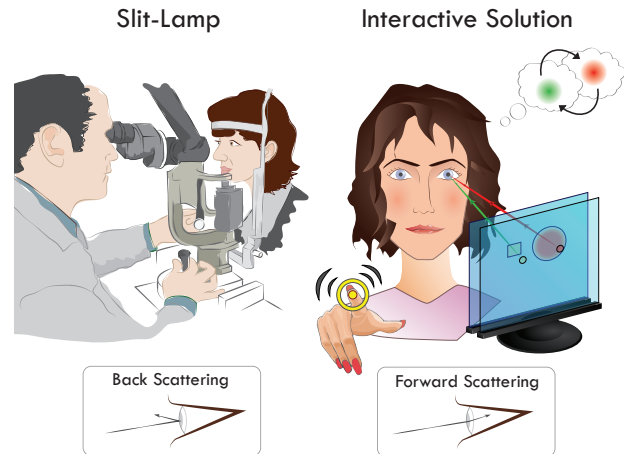


Figure 1: Can we create a device that makes people aware of their early cataract condition? Using a light-field display, our method projects time-dependent patterns onto the fovea. Interactive software measures the visibility and point spread function across sub-apertures of the crystallin lens. By repeating this procedure for several light-paths, the cataract's size, position, density, and scattering profile are estimated.

fective solution to measure optical scattering inside the human eye. Mechanically moving parts are exchanged for moving patterns, on-screen, and forego the need to use external sensors. off-the-shelf display and simple optical components make the device safe, cheap, and compact;

- Four interactive measurement techniques used to assess the size, position, attenuation, contrast, and point-spread function of scattering spots in imaging systems. These four new maps quantify and predict the scattering behavior inside the eye, and an image-based post-processing technique simulates an individual's eyesight.

The interactive measurement technique efficiently reduces the search space for the PSF map of a subject's eye. The data captured by the device is more detailed than currently known techniques. To our knowledge, this is also the first technique to simulate how individual subjects see through a cataract-affected eye.

Limitations: Since our solution requires active user participation, we are limited by the subject's ability to follow instructions. By using perceptual judgement and pattern matching, the technique does not work if a uniform-scattering cataract covers all the visible crystallin, as in advanced cases of the disease. Retinal diseases may augment the results, however, our method is highly efficient in recognizing early to mid level developments, rendering fast and simple diagnostics.

Dual-stacked-LCDs are used to create a parallax barrier device [Isono et al. 1993], which shares some limitations of other similar designs such as crosstalk, decrease in brightness, and pre-defined viewing zones [Dodgson 2009]. The map resolution is a function of pixel density, distance between LCDs screens, and the distance from the display to the eye. Current effective static contrast on LCDs may influence the ability to discern the projected patterns and measure the PSF. These limitations still allow the user to obtain reliable, repeatable results using our technology.

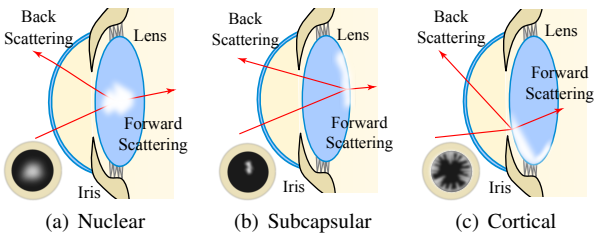


Figure 2: Most common types of cataracts: (a) Nuclear forms on the center of the crystallin, grows towards the periphery, and is strongly related to the aging process; (b) Sub-capsular starts on the back of the crystallin, mostly due to diabetes. (c) Cortical starts on the periphery, and grows inwards to its center. Back scattering reduces the visual acuity by partially blocking light. Forward scattering blurs the retinal image, decreasing contrast. Pupil size determines the strength of the effects.

1.2 Related Work in Computer Graphics

Self-Evaluation Interactive Health-care Devices: This paper complements the contributions of NETRA [Pamplona et al. 2010], but aside from using interactive techniques to eye care, there are no other pertinent similarities. It addresses a different problem, previously unexplored. NETRA measures the *required optical correction and focal range* using static clip-ons for high-resolution displays. This work computes the *spatial distribution of opacities* inside the crystallin lens and requires programmable high-contrast parallax barriers. NETRA's optics are designed to perform alignment tests, in which accommodation plays a critical role. Our approach relies on pattern matching and gaze control, where the alignment of the subject's eye is the main issue. Unlike NETRA, which has several devices providing the same final data, there is no device capable of measuring sub-aperture attenuation and contrast-sensitivity maps for a cataract affected human eye.

Glare Studies and Light-Field Techniques: Isono et al. [1993] introduced dual-stacked LCDs to achieve programmable parallax barriers. We use a similar hardware setup to handle deficiencies in the human eye. Several researchers have addressed glare removal on coded aperture cameras. Raskar et al. [2008] resampled a light field image to remove glare effect in cameras. Talvala et al. [Talvala et al. 2007] removes glare by measuring the direct and indirect lighting on the picture. Nayar et al. [Nayar et al. 2006] proposed a fast separation of direct and global components by using programmable illumination. [Kakimoto et al. 2004] formalized the glare effect through the Fraunhofer propagation. Our research focuses on an indirect component measurement and glare estimation for eyes. Hara et al. [2009] proposed the use of LCDs to block parts of the aperture which produce glare effects. Nagahara et al. [2010] used liquid crystals on silicon to create a programmable aperture camera to study its optical effects on the sensor. With our maps, and PSF, one can extend these works to correct images for cataract-affected eyes.

Simulation of a Subject's View: Several researchers have ray-traced schematic eyes in order to study the optical importance of each structure. Barsky [2004] proposed vision realistic rendering by using wavefront data to render images simulating the subject's vision. Deering [2005] used a model of the cones in the retina to simulate the perception of displayed digital images. Camp et al. [1990] developed a ray tracing technique that accounts for eye aberrations based on corneal topography. Cook et al. [1984] introduced depth of field and motion blur simulations, in ray tracing. Kolb et al. [1995] introduced the realistic camera model for computer graphics producing a variety of optical effects. Mostafawy et al. [1997] designed a virtual eye for retinal image visualization using

Features	Opacity Map	Attenuation Map	Contrast Map	Local PSFs	Scattering	Training Level
Slit Lamp	✓				Back	High
Scheimpflug	✓				Back	High
Retro Illum.	✓	✓			Fwd	Med
Shack-Hartmann	✓	✓	✓		Fwd	Low
OCTs	✓	✓			—	Med
Our Device	✓	✓	✓	✓	Fwd	Low

Table 1: Comparison of our technique against current available technologies and research tools.

ray tracing techniques. Kakimoto et al. [2007] described wavefront tracing in the eye for refractive aberrations. Loos et al. [1998] ray-traced a schematic eye for best fit progressive lenses. Machado et al. [2010] created a model for the perception of color vision deficient. Schwiegerling et al. [2000] created a diffraction model to find the acuity limit for a standard eye, while [Ritschel et al. 2009] developed a diffraction simulator to dynamically compute the PSF of a virtual eye, rendering glare effects in real-time. Although these works achieved their purpose, they did not test cataracts dysfunction; most of them are not targeted toward the simulation of an specific individual's vision. Materials to simulate cataract effects were found, but they do not account for localized scattering [de Wit et al. 2006; Fine and Rubin 1999].

2 Human Eye and Cataracts

Cataracts are denatured crystallin proteins that are clumped together in the nucleus, on the cortex or under the capsule of the crystallin (Figure 2). With the continuous production and accumulation of lens fibers throughout life, the crystallin becomes thicker and more compact. This disease is the leading cause of avoidable blindness worldwide [WHO 2005] and this occurrence is highly correlated to the aging process. 17% of the +40-year-old Americans have cataracts, 50% of +75-year-old have had cataracts, and its incidence is expected to grow with the increasing longevity [NIH-EDPRSG 2004; Li et al. 2010]. It is estimated that one third of Americans will undergo cataract surgery in their life time [Palanker et al. 2010]. There is currently no efficient method to prevent it or to completely stop its growth. The rate of this expansion, however, can be controlled if early diagnostics are obtained [Fostera et al. 2003]. Methods to detect early cataracts and assess its progression over time could be potentially helpful for the development and testing of new treatments [Asbell et al. 2005], to alert patients, and to allow lifestyle adjustments to reduce further development [Datiles et al. 2008].

Cataracts can be assessed by *backscattering* or *forward scattering* analysis (Table 1). **Backscattering examination:** A slit-lamp microscope is used to backscatter light from cataract spots. This technique, however, requires numerous focusing magnifications, angling and lighting possibilities and its reproducibility is very poor [Donnelly et al. 2004]; The Scheimpflug slit-lamp photography tilts the camera's depth of field to consistently get transversal sharp focused images of the lens. Cataract scatters light and appears as varied elevations in accordance to location and severity. Scheimpflug has the disadvantage of requiring many pictures, in different meridians, to reliably estimate the size of the opacity [Hayashi et al. 1998; Lasa et al. 1995].

Forward scattering examination: Retro-illumination techniques flood the retina with light, whose reflex reaches the crystallin from behind, propagating the scattering to the camera. Mean gray level, best fitting polynomials, feature extraction, and other image pro-

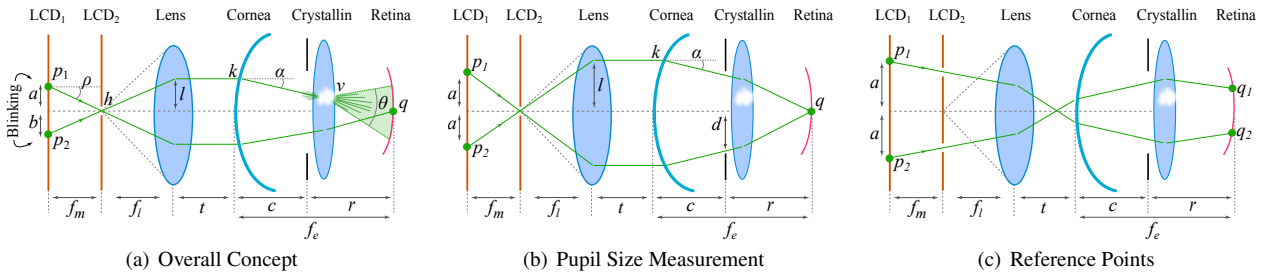


Figure 3: Cross-section of our optical setup: (a) two stacked LCD and a lens create collimated beams of light. If just a pinhole is drawn on LCD₂, the patterns displayed on LCD₁ will focus at the same spot q on the retina. Thus LCD₁ gives the brightness for each point on the retina, while LCD₂ controls the position and shape of q ; (b) Schematics for pupil size measurement. Subject chooses the biggest possible “ a ” while still seeing q ; (c) Schematics for drawing reference points and avoid eye movement and gaze. The lens is positioned at one focal length (f_l) from the display. The distance f_m defines the angular resolution.

cessing techniques are used to automatically measure size and shape of the cataract [Li et al. 2010]. Since the position of the spot is unknown, focusing skills are essential.

Research alternatives such as femtosecond lasers, and optical coherence tomography [Palanker et al. 2010] may provide new high-quality tools to estimate the size and position of a cataract. Using a Shack-Hartmann device, the coherent light ray hits the crystallin from behind and reaches the sensor. Blur captured by each lenslet is a local PSF of the lens [Donnelly et al. 2004]. Although these techniques have been successfully used for cataract surgery [Kim and Bressler 2009], their high costs limit the adoption for diagnostic purposes.

3 Scanning the Crystallin Lens

We turn a parallax barrier into a time-dependent gaze-controlled scanning mechanism in order to explore the intrinsic parameters of the human eye. Figure 3 shows a diagram of the setup in flat-land. Two stacked LCDs create a programmable parallax barrier. An additional lens in front of the display increases light efficiency and reduces diffraction, creating collimated beams that converge to the same point on the retina. The device is positioned very close to the subject’s cornea. This arrangement produces collimated beams to trace light through many regions of the crystallin (Figure 3 a), one at a time. Each beam propagates the effect of possible occluders and imperfections to the central point of the fovea. Pattern disappears on a reflective cataract spot and scatters when the ray finds a semi-transmissive spot. Based on this setup, our method computes opacity, attenuation, contrast, and PSF maps of the eye using interactive pattern-matching functions, which compare clear-path light beams and scattered ones. We have discarded a tridimensional tomography-like analysis since the relaxed crystallin is only 4mm-thick, on average.

Intuition of our design relies on the role of each LCD: each pixel on LCD₁ maps to a region on the crystallin and each pixel on LCD₂ corresponds to a retinal position. Patterns drawn on LCD₂ are reflected on the retina, while the brightness of all on LCD₁ are integrated on the same retinal point. A central pinhole in LCD₂ is enough to trace rays to a foveal spot. Position p_1 (Figure 3(a)) inside the crystallin is then a function of the angle ρ :

$$v(\rho) = f_l \tan \rho - c \tan \alpha, \quad (1)$$

where the bending angle α is defined by the optical corneal power in the point k . To create patterns on the subject’s view, however, the pinhole on LCD₂ changes to the desired pattern. The position h on LCD₂ is mapped to the retina as (derived from compound lens equation):

$$q(h) = \frac{(-f_e^2 - f_e f_l)h}{f_l(-f_e - f_l + f_e t)} \quad (2)$$

Figure 4 illustrates our interactive method. By measuring the pupil size, which defines the discretization of the pupil area and enables the computation of the cataract size in meaningful physical units, we sequentially scan the subject’s crystallin to identify the presence of cataracts. If this is found to be true, the subject identifies the position of opacities and in a posterior step measures the light attenuation for each sub-aperture of the eye, thus creating opacity and attenuation maps. Measured attenuation values estimate the intensity of the local PSF peak. The subject then performs perceptual pattern matching to measure the tail of the PSF. If the attenuation value is small, the tail may be bigger than the fovea, and its direct measurement is not reliable. Contrast-sensitivity tests, described later, give us an approximation for the PSF. For each step of the test, the user’s role is to match patterns which are projected onto the fovea.

Estimating Pupil Size: Figure 3(b) shows a simplified ray diagram to measure pupil size with two light beams in flatland. In practice we display circular-arranged patterns p_i with radius a . Parallel rays enter the eye and converge to a single point q on the fovea. Via interactive software, the subject increases a up to a point where the patterns disappear (Figure 4 a). Pupil radius is then given by $d = a - c \tan \alpha$, where c is the distance from the cornea to the crystallin. We assume a circular pupil, thus the search is 1D.

2D Scanning for the Opacity Map: By subdividing the crystallin into testing regions, according to the pixel density of the LCD stack and pupil size, we draw a single dot p_1 on LCD₁ and a pinhole on LCD₂. Given the pupil size, we move p_1 to cover the visible crystallin (Figure 4 b). This first evaluation identifies whether or not there is cataract. If the subject sees the pattern fading or disappearing, the software slows the scanning, allowing the user to mark faded positions (Figure 4(c)). We use audio feedback (beeps) for each new position. An opacity map is built by concatenating the visibility functions for each sub-aperture of the crystallin.

Brightness Match for the Attenuation Map: The attenuation map measures the relative light attenuation across the crystallin. LCD₁ shows a pair of alternating dots (Figure 3 a). p_1 is computed as the farthest point on the opacity map from the cataract spots. p_2 is a marked spot on the opacity map. Since both are projected on q at different time-slices, the subject sees similar patterns with oscillating brightness. At this point, the subject decreases the intensity level of p_1 until the oscillation stops (Figure 4 d). This same task is executed for all marked regions on the opacity map. In the end, the attenuation map is built, showing the relative density of the cataracts.

Point Spread Function Matching: Just like in the brightness test, the subject compares and matches alternating patterns (Figure 4(f)). Two patterns are drawn on LCD₂. The former is a single pixel stimulus that hits the cataract spreading light onto the retina. The

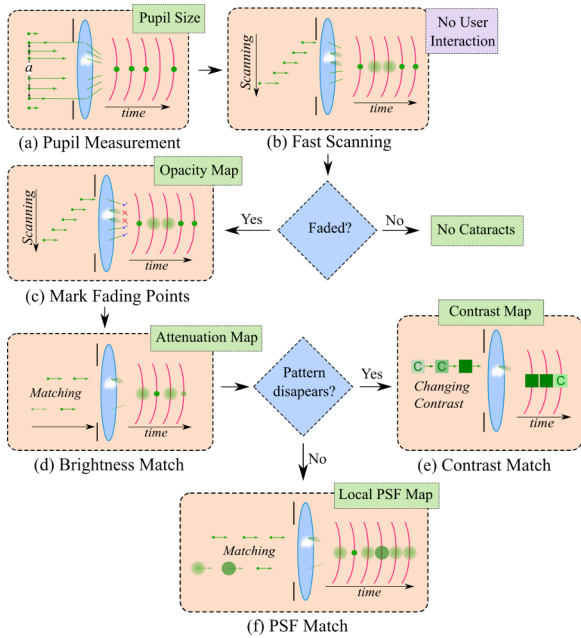


Figure 4: Overall hierarchical method to efficiently measure cataracts. (a) Subject measures pupil size by increasing the distance a while perceiving the green dot. (b) Software automatically scans the lens to check for the presence of cataracts. (c) If a scattering spot is found, the scanning procedure is repeated with the subject’s feedback. (d) By matching the brightness of two alternating paths of light we compute an attenuation map. (e) For a high scattering spot, the local contrast-sensitivity test replaces the local PSF measurement. In this case the subject increases the contrast of the displayed pattern up to a point where the letter becomes discernible. (f) Local PSF matching is the most detailed mapping, where the peak and Gaussian spread are measured for each scattering spot. The four maps together summarize the forward scattering effects of cataracts.

latter is a Gaussian-box function which describes a local PSF:

$$c(x) = \beta g(\sigma, x) + (1 - \beta) * p(x), \quad (3)$$

where β is the scaling factor defined by the measured attenuation value, g is a normalized Gaussian function and p is a normalized box function. In the absence of blur, $\beta = 0$. For each marked spot on the opacity map, the subject changes the values of β and σ to best match the visualized PSF.

Contrast-Sensitivity Test: A contrast sensitivity test is a replacement for the PSF measurement procedure. Wider PSFs project their tail out of the fovea and thus the subject may not be able to reliably measure it. A pixel is rendered on LCD_1 for each attenuated sub aperture, as well as the contrast test pattern on LCD_2 , until a square is observed. The subject then presses buttons to increase the contrast until the rotated letter 'C' becomes visible (Figure 4)(e). 'C' is then marked and noted. This visual acuity test is repeated for each sub-aperture, generating a complete map in the end.

3.1 Implementation Details

Gaze Control and Eye Position: Since all collimated beams are projected onto the fovea, no matter from which part of the cornea they enter the eye, the subject keeps looking to the same point and does not gaze. However, the subject can shift by the width of the pupil diameter, and remain seeing the same image. In order to overcome this, and keep the user in the same place, we draw reference points (Figure 3 c) as a circular arrangement of patterns on LCD_2 .

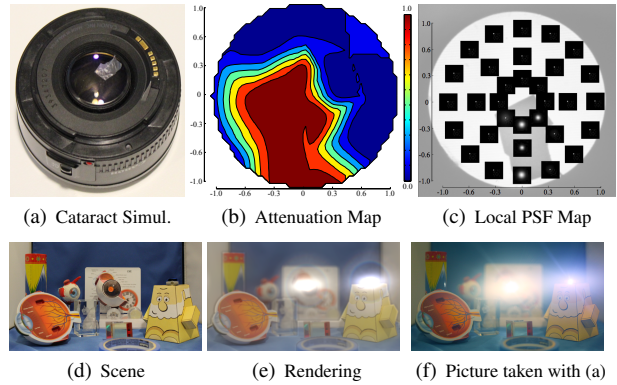


Figure 5: We simulate strong cataracts by adding an 80-degree diffuser behind a 55mm lens of an SLR camera (a). We estimated an attenuation map for an aperture of 2.2cm and (b) local PSFs map for aperture of 3cm. The cataract PSF is applied on the picture (d). The rendered image (e) shows similar effects as the picture taken with the cataract-simulated lenses (f).

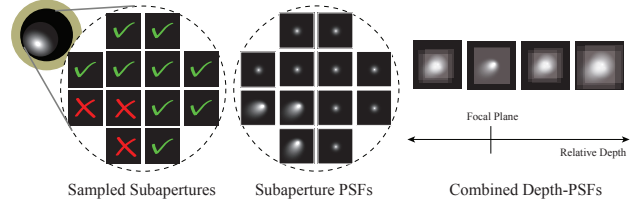


Figure 6: Composition of lens’ depth-dependent PSFs as the sum of all sub-aperture PSFs, shifted and combined in accordance with the relative depth from focal plane and the lens aperture

Part of the circle disappears when the subject moves beyond a certain limit. With this technique, the subject can detect when they are off center, and should return to the original position.

System Resolution: Assuming h is a pinhole, the size of the cross section defined by the collimated light beams between the lens and the cornea is given by $s(p) * f_l / f_m$, where $s(p)$ is the radius of the pattern p on LCD_1 . Thus the bigger f_m , the smaller the beam is. Discretizations of the crystalline and the retina are defined by the angle ρ (Equation 1) and by the pixel size of LCD_2 (Equation 2), respectively.

Handling Accommodation and Refractive Errors: Our design does not allow for multi-focus. We do not assemble an image on the subject’s retina as the standard parallax barrier does. An additional lens plays an important role in handling accommodation. Subjects can focus on LCD_2 just like any other object seen through a lens. Refractive errors add a small variance to the position of the patterns on the retina, and are enough to make the subject gaze, thus adding some small uncertainty to the computation of the position of the cataract in the crystalline (e.g., if the scanning runs in circles and the subject has astigmatism, the method measures ellipses).

4 Rendering the Subject’s View

We propose an image-based approach for simulating the vision of a specific individual affected by cataracts. A depth-accommodation-dependent convolution of sub-aperture PSFs simulates the view of a cataract-affected eye. We convolve depth-masked patches of the input image with their corresponding PSFs and combine the results into the final image. Each depth-based PSF is computed by combining the sub-aperture PSFs, which are given by the scattering profile of an eye lens, as described in Section 3. Figure 6 illustrates



Figure 7: Rendering features: a) "Bokeh" effect, the cataract shape projected from out-of-focus bright light sources; b) the simulated cataract on the lens; c) the opacity map; d) the PSF map; Cataract spots scatter a lot of light, appearing as a projected pattern around out-of-focus bright light sources, also generating large glare patterns.

327 how local PSFs from sub-apertures of a lens are combined through
 328 all depths. At the focal plane, all local PSFs are just superposed
 329 and added, averaging their values. At depths away from the focal
 330 plane, the local PSFs are shifted from the center according to the
 331 distance to the focal plane, and the aperture, given by the pupil di-
 332 ameter. Computation of these depth-dependent PSFs can be defined
 333 by Equation 4:

$$PSF(A, B) = \int PSF_i + B \vec{g}_i \partial i \quad (4)$$

344 where B is the depth-offset in diopters (reciprocal of the focal
 345 length) from the plane of focus defined by the accommodation A ,
 346 \vec{g}_i is the vector that represents the shift of a sub-aperture s_i from the
 347 center of the lens, and PSF_i is s_i 's PSF. The product of B and \vec{g}_i
 348 model how the circle of confusion projected through s_i gets shifted
 349 from the center of the image as a function of depth. The final image
 350 is given by the integration of the depth-masked patches convolved
 351 with their respective PSFs:

$$IMG(A) = \int h(B) \otimes PSF(A, B) \partial B \quad (5)$$

342 Where $h(B)$ gives the depth-masked patch of the input image I and
 343 is defined pixel-wise by:

$$h_{x,y}(B) = \begin{cases} I_{x,y} & \text{if } depth(I_{x,y}) = B \\ 0 & \text{otherwise} \end{cases} \quad (6)$$

344 where $I_{x,y}$ is the intensity of the pixel x, y . Given sub-aperture
 345 PSFs, this depth-based approach renders artifacts which are simi-
 346 lar to those described by cataracts-affected subjects, also comput-
 347 ing the expected depth-of-field. To account for diffraction from
 348 the pupil, lens fibers and cataract opacities, we also added an aug-
 349 mented version of the glare model described in [Ritschel et al.
 350 2009] to the computed PSF, including the attenuation map as a mul-
 351 tiplication step to the proposed aperture model. Figure 7 shows a
 352 simulated night-driving scene with the experimental data used to
 353 render it. Cataract shape (b) can be seen as a mask on the "bokeh"
 354 effect of the PSF composition.

355 5 Prototypes and Evaluation

356 We explored different designs that span across size, materials, in-
 357 terface, cost and static contrast. Figure 8 shows three of our pro-
 358 tootypes. Our *Dual-LCD Monitor* is build using two 18" LCD TFT
 359 monochrome medical monitors stacked $f_m = 24mm$ apart, with
 360 brightness of $700cd/m^2$, contrast ratio of 550 : 1 and 90DPI

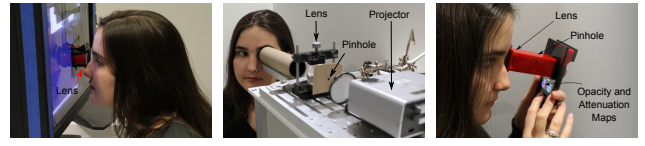


Figure 8: Three prototypes: (a) stack of two LCDs from high-contrast low-resolution monochrome medical monitors; (b) a high-contrast DLP projector plus a pinhole mask and (c) the cell phone LCD plus a pinhole mask. Because of the absence of color filters, high contrast ratio and a better light box than standard LCDs, we consider (a) our best overall setup. (b) brightest and highest-contrast setup, which allow meaningful scattering projection through high density cataracts; and (c) it is the most portable, comprising of a clip-on for smart-phones.

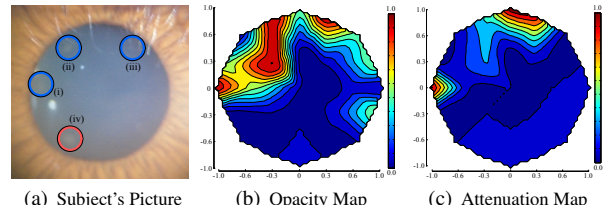


Figure 9: Opacity and attenuation maps for one subject. (a) Picture of the cataract-affected eye. (b) Linear interpolated opacity map showing scattering regions highlighted by (i), (ii) and (iii). Spot (iv) cannot be found in our measurements. Attenuation map (c) matches the opacity map and reveals a required increase of 70% on the red parts to allow the subject to observe the same intensity as a beam going through the center of eye. Subject was asked to rest between opacity and brightness matching tests, requiring a re-alignment of their position using the reference points.

361 (280 μm pixel pitch). On top of the stack, a 20-diopter lens (Figure
 362 8 a). The scanning resolution is 461 μm on the crystallin. Since
 363 they do not have color filters, the aberrations are smaller than tradi-
 364 tional monitors and the high contrast gives a smaller residual light
 365 level for black pixels.

366 Replacing LCD_2 by a pinhole mask, we create a cheaper version
 367 of the same optics, which is still capable of measuring the opac-
 368 ity and attenuation maps, but cannot measure the contrast map or
 369 point spread functions. This setup can be implemented as a clip-on
 370 for any high-contrast spatial light modulator. The *DLP Projector*
 371 prototype consists of a Mitsubishi PK10 pocket projector (DMD),
 372 a 50 × 40mm diffuser as projection screen, a 16-diopter lens, and
 373 a pinhole with radius of 100 μm , producing a scanning resolution
 374 of 47 μm on the crystallin (Figure 8 b.). *Cell phone* setup uses a
 375 Samsung Behold II (180DPI or 141 μm on pixel pitch - Figure 8 c
 376), with a static 100 μm pinhole, 40mm from the display, and a 25-
 377 diopter lens. The scanning resolution is 138 μm on the crystallin.

378 5.1 Controlled Evaluation

379 Our methods are evaluated using a camera focused at infinity, with
 380 diffusers placed at the lenses, as shown in Figure 5 (a). We manu-
 381 ally match the patterns seen through a live-view on a PC
 382 connected to the camera and find the parameter required for opti-
 383 mal matching. Each level of our method is validated indepen-
 384 dently of the others. For the accuracy tests, our maps are com-
 385 pared against pictures taken in each estimated position for attenu-
 386 tion and PSF maps. For each round, diffusers were randomly cho-
 387 sen. Canon 5D Mark II with 50mm lens, and C-mount Flea camera
 388 from Point Grey Research with 16mm lens are used. Luminit dif-
 389 fusers with scattering angles of 5° (7x3mm), 30° (9x4mm) and

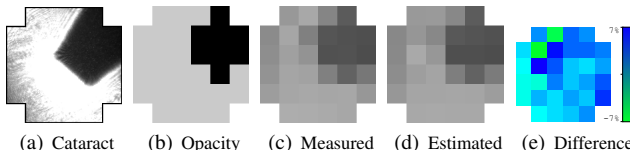


Figure 10: Attenuation comparison for an entire round. Each pixel represents one estimation. (a) Shows the simulated cataract; (b) the estimated opacity map (c) pictures of each measurement spot; (d) estimated attenuation map and (e) difference between measured and estimated in 8-bit scale.

440 reliability performed because of low-quality slit-lamp pictures. All
441 tests were made using reference points to avoid eye motion (Figure
442 3 c).

443 For these experiments, we assume no optical aberrations (the person
444 takes the test wearing his corrective lenses, if (s)he uses some) and
445 a thin lens system. Thus, α in Equation 1 can be approximated by
446 $\tan \alpha = l/f_e$, where f_e is the focal length (axial length) of the eye,
447 which is the reciprocal of the optical power at point k . $c = 0.5\text{mm}$
448 in our calculations.

449 6 Discussion and Conclusion

450 We proposed an interactive method coupled with an optical design
451 to detect early cataracts in the human eye using view-dependent
452 high-contrast displays. This innovation measures the forward scat-
453 tering profile and creates the PSF of the crystallin with no need
454 of a coherent light source and no mechanical apparatus. The de-
455 sign ensures the projection of pattern directly onto the fovea to
456 avoid gazing issues. Users look through an eyepiece and interact
457 with a keypad based on what they see. Our interactive method
458 scans the subject's crystallin lens to estimate opacities, attenu-
459 ation levels, contrast-sensitivity, and local point-spread functions.
460 Validation experiments attested the precision and accuracy of the
461 method, accommodation, and gaze control of the optical design of
462 the prototypes. We believe our attenuation, contrast, and PSF maps
463 are unique, and no currently available device produces comparable
464 data. Repeatability, and the complete absence of false positives, are
465 incentives to continue this investigative research.

466 Simple presence of opacities might already indicate glare issues,
467 but a complete contrast, or PSF map, can give a more detailed
468 profile of the effects on scenes with high dynamic ranges. A PSF
469 mapping tool provides a new opportunity for doctors and patients.
470 Renderings help to mitigate this relationship through a shared vi-
471 sual experience, reinforced by our unique mapping solution, open-
472 ing a dialogue to further assess and aid the diagnosis of developing
473 cataracts.

474 **Cataract-induced contact lenses:** One subject had his contact
475 lenses scratched in a zig-zag-line pattern with thickness of 0.5mm .
476 Subject generated 10 opacity and attenuation maps. Estimated size
477 is 0.57mm using our method. Repeatability is $0.15\text{mm}^2 \pm 0.13$ in
478 size and $0.31\text{mm} \pm 0.13$ in the position of the simulation's center
479 of mass. Average result of the 10 attenuation maps indicates a re-
480 quired increase of 131% in brightness for the points going through
481 the scratch. The absolute average difference is $6.8\% \pm 5.2\%$. Mea-
482 surements were taken under a pupil radius of 1.32mm . The con-
483 tact lens can rotate when the subject blinks during the test. All tests
484 were made using reference points shown in Figure 3 (c) to avoid
485 eye motion.

486 **Experiences shared on the user studies:** Many of the test sub-
487 jects were fascinated by their opacity map on the screen of a smart-
488 phone. One of the cataract-affected subjects has reported difficulty
489 in explaining the visual effects to his family. A simple rendering
490 tool may address these communication issues between them. Re-
491 sponse from the local community has been great. Our data shows
492 a reasonable repeatability, but some users found the alignment task
493 difficult to understand. The owner of a respectful company that
494 provides health care in developing countries has demonstrated ex-
495 citement about the technology: "Village health workers will be able
496 to cheaply and quickly flag early stage cataracts and macular degen-
497 eration in order to refer individuals to hospitals, where their vision
498 can be restored before they effectively become blind".

499 **Reactions from ophthalmologists:** Several research and local
500 practicing ophthalmologists have been in collaboration with this
501 project, and are enthusiastic about its unique outcomes. Many of
502 them have experimented with the device, and the general response
503 has reinforced that reliable quantitative measurements for cataracts
504 are already very helpful for screening purposes. One of them com-
505 mmented on their experience that the Shack-Hartmann wavefront
506 sensor to measure high-order optical distortions of the human eye
507 had no practical application twenty years ago. Today, the high ac-
508 curacy of these devices provide the only reliable data for the LASIK
509 surgery. Widespread availability of devices like ours, which gener-
510 ate quantitative data about cataracts, may benefit the future of di-
511 agnostic and surgical practice. Since cataracts are highly correlated
512 with macular degeneration, many doctors have suggested the use of
513 this device as a side screening tool for other visual impairments.

390 80° ($9 \times 4\text{mm}$) and a piece ($9 \times 6\text{mm}$) of a diffuse plastic bag are
391 tested. Figure 5 shows the attenuation and point-spread-function
392 maps for a simulated cataract and its respective visual effects.

393 We test the accuracy of the estimated attenuation maps using the
394 *DLP Proj. plus Mask* with the Flea Camera. Pictures of the scat-
395 tered and free-path light beam were taken before the user adjusts the
396 brightness levels. For 289 measurement spots in 7 rounds randomiz-
397 ing diffusers, the accuracy of the attenuation levels in absolute
398 average error is $1.03\% \pm 4.20\%$.

399 Contrast-sensitivity maps were estimated using the *Dual-LCD*
400 *Monitor* with the Canon 5D. The repeatability of the contrast value
401 (Range [0, 1]) has an average error of 0.03 ± 0.03 for 116 measure-
402 ments on 4 rounds.

403 PSFs maps were computed for the 80° and 5° diffusers. Using
404 the Dual-LCD Monitor with a Canon 5D, the repeatability of the
405 measurements in 128 tests points (4 rounds) is 0.03 ± 0.13 in
406 normalized scale. PSF maps also represent position and size of
407 a cataract. Repeatability for the position of the diffuser's center
408 of mass is $0.01\text{mm} \pm 0.007$. The 80° of 36mm^2 was measured
409 having 34mm^2 with an average error of 4.27mm^2 and the 5° of
410 21mm^2 having 29mm^2 , with an average error of 8.55.

411 **Cataract-induced contact lenses:** One subject had his contact
412 lenses scratched in a zig-zag-line pattern with thickness of 0.5mm .
413 Subject generated 10 opacity and attenuation maps. Estimated size
414 is 0.57mm using our method. Repeatability is $0.15\text{mm}^2 \pm 0.13$ in
415 size and $0.31\text{mm} \pm 0.13$ in the position of the simulation's center
416 of mass. Average result of the 10 attenuation maps indicates a re-
417 quired increase of 131% in brightness for the points going through
418 the scratch. The absolute average difference is $6.8\% \pm 5.2\%$. Mea-
419 surements were taken under a pupil radius of 1.32mm . The con-
420 tact lens can rotate when the subject blinks during the test. All tests
421 were made using reference points shown in Figure 3 (c) to avoid
422 eye motion.

423 5.2 User Evaluation

424 18 subjects tested our prototype based on a cell-phone display.
425 Each subject took the test twice for training, and at least twice for
426 data collection. Each map measures the observed attenuation for
427 24 testing points. A group of 5 early cataract-affected volunteers
428 (ages 68 to 76 and one 30-year-old) took the initial scanning pro-
429 cedure. Estimated total size for their cataracts is $1.46, 0.86, 0.82,$
430 0.46 and 0.34mm^2 . Their average error in position is $0.18\text{mm} \pm$
431 $0.01, 0.43\text{mm} \pm 0.18, 0.40\text{mm} \pm 0.15, 0.60\text{mm} \pm 0.36$ and
432 $0.32\text{mm} \pm 0.10$, and in size is $0.08\text{mm}^2 \pm 0.01, 0.11\text{mm}^2 \pm 0.09,$
433 $0.17\text{mm}^2 \pm 0.10, 0.27\text{mm}^2 \pm 0.14$ and 0 respectively. 2 early
434 cataract-affected volunteers took the brightness matching test. Av-
435 erage error is $12.2917\% \pm 0.01\%$ and $6.38\% \pm 3.64\%$. Figure 9
436 shows the estimated opacity and attenuation maps for a volunteer
437 compared with a picture of his eye. Additionally, 14 healthy eyes
438 were scanned and no cataract was found. Quantitative accuracy
439 tests comparing our maps against slit-lamp pictures could not be

A few ophthalmologists we have been discussing with, reported strong concerns about the complete absence of a glare disability test in order to obtain a driver's license. For instance, visual acuity tests, in general, do not assess for glare and night driving effects, while simple and cheap tests such as ours, would reveal currently unchecked impairments. Our overall goal is to create tools that empower self-awareness about commonly unscreened health condition of the eye. We stress that this device does not directly diagnose or treat for cataracts, but in the future, methods like this might be able to give a complete summary of visual performance. Our hope is that these results encourage more people to design and develop interactive tools which will augment the understanding of the human visual experience.

References

- ASBELL, P. A., DUALAN, I., MINDEL, J., BROCKS, D., AHMAD, M., AND EPSTEIN, S. 2005. Age-related cataract. *The Lancet* 365 (9459), 599–609.
- BARSKY, B. A. 2004. Vision-realistic rendering: simulation of the scanned foveal image from wavefront data of human subjects. In *APGV 2004*, ACM, 73–81.
- CAMP, J., MAGUIRE, L., AND ROBB, R. 1990. An efficient ray tracing algorithm for modeling visual performance from corneal topography. In *Visualization in Biomedical Computing, 1990. Proceedings of the First Conference on*, 278–285.
- CAMPARINI, M., MACALUSO, C., REGGIANI, L., AND MARAINI, G. 2000. Retroillumination versus reflected-light images in the photographic assessment of posterior capsule opacification. *IOVS* 41, 10, 3074–3079.
- COOK, R. L., PORTER, T., AND CARPENTER, L. 1984. Distributed ray tracing. *SIGGRAPH Comput. Graph.* 18 (January), 137–145.
- DATILES, M. B., ANSARI, R. R., SUH, K. I., VITALE, S., REED, G. F., JR, J. S. Z., AND FERRIS, F. L. 2008. Clinical detection of precataractous lens protein changes using dynamic light scatterin. *Arch. Ophthalmol.* 126(12), 1687–1693.
- DE WIT, G. C., FRANSSEN, L., COPPENS, J. E., AND VAN DEN BERG, T. J. 2006. Simulating the straylight effect of cataracts. *J. Cataract Refract Surg.* 32, 294–300.
- DEERING, M. F. 2005. A photon accurate model of the human eye. In *SIGGRAPH 2005*, vol. 24(3), 649–658.
- DODGSON, N. 2009. Analysis of the viewing zone of multi-view autostereoscopic displays. In *SPIE Stereoscopic Displays and Applications XIII*, 254265.
- DONNELLY, W. J., PESUDOVS, K., MARSACK, J. D., SARVER, E. J., AND APPLEGATE, R. A. 2004. Quantifying scatter in shack-hartmann images to evaluate nuclear cataract. *Journal of refractive surgery* 20(5), S515–S522.
- FINE, E. M., AND RUBIN, G. S. 1999. Effects of cataract and scotoma on visual acuity: A simulation study. *Optometry and Vision Science* 76(7), 468–473.
- FOSTERA, P. J., WONG, T. Y., MACHIN, D., JOHNSON, G. J., AND SEAH, S. K. L. 2003. Risk factors for nuclear, cortical and posterior subcapsular cataracts in the chinese population of singapore. *Br J Ophthalmol* 87, 1112–1120.
- HARA, T., SAITO, H., AND KANADE, T. 2009. Removal of glare caused by water droplets. In *Proceedings of the 2009 Conference for Visual Media Production*, IEEE Computer Society, Washington, DC, USA, CVMP '09, 144–151.
- HAYASHI, K., HAYASHI, H., NAKAO, F., AND HAYASHI, F. 1998. In vivo quantitative measurement of posterior capsule opacification after extracapsular cataract surgery. *Am J Ophthalmol* 125, 837–843.
- ISONO, H., YASUDA, M., AND SASAZAWA, H. 1993. Autostereo-scopic 3-d display using lcd-generated parallax barrier. *Electr. and Comm. in Japan* 76(7), 7784.
- KAKIMOTO, M., MATSUOKA, K., NISHITA, T., NAEMURA, T., AND HARASHIMA, H. 2004. Glare generation based on wave optics. *CG&A* 0, 133–142.
- KAKIMOTO, M., TATSUKAWA, T., MUKAI, Y., AND NISHITA, T. 2007. Interactive simulation of the human eye depth of field and its correction by spectacle lenses. *Comp. Graph. Forum* 26, 627–636.
- KIM, S., AND BRESSLER, N. M. 2009. Optical coherence tomography and cataract surgery. *Curr Opin Ophthalmol* 20(1) (Jan), 46–51.
- KOLB, C., MITCHELL, D., AND HANRAHAN, P. 1995. A realistic camera model for computer graphics. In *ACM SIGGRAPH '95*, 317–324.
- LASA, M., DATILES, M., MAGNO, V., AND MAHURKAR, A. 1995. Scheimplug photography and postcataract surgery posterior capsule opacification. *Ophthalmic Surg.* 26, 110–113.
- LI, H., LIM, J. H., LIU, J., MITCHELL, P., TAN, A. G., WANG, J. J., AND WONG, T. Y. 2010. A computer-aided diagnosis system of nuclear cataract. *IEEE Trans. Bio. Eng.* 57(7).
- LOOS, J., SLUSALLEK, P., AND SEIDEL, H.-P. 1998. Using wavefront tracing for the visualization and optimization of progressive lenses. *Comp. Graph. Forum* 17, 255–265.
- MACHADO, G. M., AND OLIVEIRA, M. M. 2010. Real-time temporal-coherent color contrast enhancement for dichromats. *Comp. Graph. Forum* 29, 3, 933–942.
- MOSTAFAWY, S., KERMANI, O., AND LUBATSCHOWSKI, H. 1997. Virtual eye: Retinal image visualization of the human eye. *IEEE CGA* 17, 8–12.
- NAGAHARA, H., ZHOU, C., WATANABE, T., ISHIGURO, H., AND NAYAR, S. K. 2010. Programmable aperture camera using lcos. In *ECCV'10*, Springer-Verlag, Berlin, Heidelberg, 337–350.
- NAYAR, S., KRISHNAN, G., GROSSBERG, M. D., AND RASKAR, R. 2006. Fast Separation of Direct and Global Components of a Scene using High Frequency Illumination. *ACM TOG* 25, 3, 935–944.
- NIH-EDPRSG. 2004. Prevalence of cataract and pseudophakia/aphakia among adults in the united states. *Arch Ophthalmol* 122.
- PALANKER, D. V., BLUMENKRANZ, M. S., ANDERSEN, D., WILTBERGER, M., MARCELLINO, G., GOODING, P., ANGELEY, D., SCHUELE, G., WOODLEY, B., SIMONEAU, M., FRIEDMAN, N. J., SEIBEL, B., BATLLE, J., FELIZ, R., TALAMO, J., AND CULBERTSON, W. 2010. Femtosecond laser-assisted cataract surgery with integrated optical coherence tomography. *Science Translational Medicine* 2, 58, 58ra85.
- PAMPLONA, V. F., MOHAN, A., OLIVEIRA, M. M., AND RASKAR, R. 2010. Netra: interactive display for estimating refractive errors and focal range. *ACM Trans. Graph.* 29, 4, 77:1–77:8.
- RASKAR, R., AGRAWAL, A., WILSON, C. A., AND VEERARAGHAVAN, A. 2008. Glare aware photography: 4d ray sampling for reducing glare effects of camera lenses. In *ACM SIGGRAPH 2008 papers*, 56:1–56:10.
- RITSCHEL, T., IHRKE, M., FRISVAD, J. R., COPPENS, J., MYSZKOWSKI, K., AND SEIDEL, H.-P. 2009. Temporal glare: Real-time dynamic simulation of the scattering in the human eye. *Comp. Graph. Forum* 28, 2, 183–192.
- SCHWIEGERLING, J. 2000. Theoretical limits to visual performance. *Survey of ophthalmology* 45, 2, 139–146.
- TALVALA, E.-V., ADAMS, A., HOROWITZ, M., AND LEVOY, M. 2007. Veiling glare in high dynamic range imaging. vol. 26.
- WHO, 2005. State of the world's sight: Vision 2020, the right to sight: 1999–2005.